Supplemental Text

S1. Validation of simulated irrigation water withdrawal

The global distribution of the mean annual irrigation water requirement is shown in Figure S1 (b). The geographical pattern agreed well with the results of earlier studies (e.g., Figure 5 of Döll and Siebert, 2002; Figure 4 of Wada et al., 2011). It is concentrated in western South Asia, northern China, and central and western USA. The simulated and reported national irrigation water withdrawals are compared in Figure S2. We referred to the national agricultural water withdrawal reported in AQUASTAT (www.fao.org/nr/aquastat/) for the year of 2000. For the four main countries that used a large volume of irrigation water, namely, India, China, USA, and Pakistan, the simulation agreed fairly well with the AQUASTAT estimation. For the remaining countries, although there was a large spread, the simulated values rarely exceeded more than double or less than half of the estimation in AQUASTAT. We found a general tendency to overestimate irrigation withdrawals in the major countries, while there was an underestimation in the other countries. The reasons for this have not yet been established because a numbers of factors influence the simulation results.

S2. Validation at selected basins

S2.1 River discharge in the less heavily human-affected river basins.

The results of river discharge simulations in the less heavily human-affected river basins are shown in Figure S3. For the river basins in the tropics, the performance varied by basin. The river discharge simulation of the Amazon River at Obidos had a very good agreement between the observation and simulation (Fig S3 a). In contrast, the discharge of the Congo River at Kinshasa was overestimated by a factor of two, but the seasonality (i.e., the timing of peak discharge and shape of the hydrograph) agreed well with the observation. In both basins, human activity has had little effect; hence, the results of the ALL and NAT simulations overlapped.

For the river basins in subarctic climates, the simulations had a common tendency to underestimate the annual river discharge and the amplitude of seasonal variation. For the Yenisei River, the river discharge was well reproduced in the dry months, but was substantially underestimated in the wet months (Fig. S3 c). For the Ob River, the mean annual and inter-annual variation in river discharge was well simulated, but the amplitude of the seasonal variation was much smaller than the observation. The simulated river discharge underestimated in wet months and overestimated in dry months (Fig. S3 d). The Lena and the Amur Rivers had a similar tendency to that seen in the Yenisei and Ob, respectively (Fig. S3 e-f). Although a large number of major reservoirs are located in these basins, the influence of these human activities did not have a large effect on the simulation results; hence, the results of ALL and NAT simulations in Fig, S3 (c-e) overlap to a large extent.

S2.2 TWS in less heavily human-affected basins

Human activity has a negligible impact on the TWS in the Amazon and Congo rivers (Fig. S4a and S4b respectively). The TWSA in these two rivers only reflects the variations in natural hydrological components, namely, soil moisture, renewable groundwater, and river water. Among these three components, river channels provided the predominant water storage in these basins, which was consistent with the findings of Kim et al. (2009).

There is little human settlement along the three rivers investigated in Siberia, namely the Yenisei, Ob, and Lena Rivers (Fig. S4 c-e). These basins are characterized by the accumulation and thawing of snow and a considerable volume of the reservoir storage is used to produce hydropower. For the Yenisei, Ob, and Lena rivers, the simulated monthly peak of the TWSA was a month earlier than the GRACE observation. Because the predominant TWS component of these basins is snow, the results indicate that in H08 snow thaws earlier than the observation. The model estimated the inter-annual trend of TWSA fairly well

in the Amur River, but it failed to reproduce the intra-seasonal variations, which are substantially smaller than in other basins (Fig. S4 f).

S3. Validation of reservoir operation simulations

The reservoir operation sub-model of H08 was first proposed in Hanasaki et al. (2006) as an independent model, then incorporated into the H08 model (Hanasaki et al., 2008a,b). The sub-model was extensively validated in Hanasaki et al. (2006) for 28 reservoirs worldwide, but due to the limited availability of long-term global meteorological data at the time of the study, the simulation and validation period was only two years (1987-1988). Here, we validated the operation of four selected reservoirs where long-term operation records were available.

The reservoir operation sub-model generates the operation rules of individual reservoirs. For reservoirs where irrigation water supply is not the primary purpose, the daily release is as follows:

$$r' = \bar{\imath} \qquad (S1)$$

where r' is the targeted daily release [kg s^{-1}] and $\bar{\imath}$ is the mean annual inflow into the reservoir. The formulation indicates that reservoir operation removes the temporal variation in river inflow and water is released constantly at the rate of the mean annual inflow. For reservoirs where irrigation water supply is the primary purpose, the daily release is as follows:

$$r' = \begin{cases} \frac{\bar{\imath}}{2} \times \left(1 + \frac{\sum_{area} k_{alc} \times d}{\sum_{area} k_{alc} \times \bar{d}}\right) & \left(\bar{d} \geq \frac{\bar{\imath}}{2}\right) \\ \bar{\imath} + \sum_{area}\{k_{alc} \times (d - \bar{d})\} & \left(d < \frac{\bar{\imath}}{2}\right) \end{cases} \qquad (S2)$$

where d and $\bar{d}$ are the daily and the mean annual water requirement in the lower stream. The term Σarea indicates integration over the grid cells downstream of each reservoir. The downstream included the reach down to the next reservoir, or if there were no further reservoirs, down to the river mouth. We set the maximum distance as 10 grid cells below the reservoir. k_{alc} is proportional to the mean annual inflow from upstream reservoirs, and k_{alc} is 1 if the grid point has only one irrigation reservoir upstream. The formulation indicates that the reservoir operation adds the temporal variation, which is harmonized with the water requirement in the lower reach.

Then, the daily release from reservoir (r) [kg s^{-1}] is expressed as follows:

$$r = \begin{cases} k_{rls} \times r' & (0.5 \leq c) \\ \left(\frac{c}{0.5}\right)^2 k_{rls} \times r' + \left\{1 - \left(\frac{c}{0.5}\right)^2\right\} i & (c < 0.5) \end{cases} \qquad (S3)$$

where k_{rls} is the release coefficient [-], which is expressed as $k_{rls} = S_{first}/0.85C$ or the ratio of reservoir storage at the beginning of the first year of operation (S_{first}) and 85% of the total storage capacity (C). c [-] is the normalized storage capacity, which is expressed as $c = C/\bar{I}$ or the ratio of reservoir capacity [kg] to the mean annual total inflow [kg]. The formulation indicates that release is identical to the daily targeted release, but it reflects the storage condition of the first year of operation. If the storage is more than 85% of the capacity, the volume released is more than the targeted storage, to reduce the storage. In the opposite case, the release is less than the targeted storage, to recover the storage. For reservoirs with storage capacity less than 50% of the mean annual inflow, due to their limited capacity to control the inflow, the release reflects the inflow condition.

Figure S5 (a) shows the simulation results for the Fort Peck Dam, which is located in the upper Missouri River in the USA. For this case, the inflow agreed well with observations in terms of mean annual inflow and inter-annual variations. Both the historical variations in storage and release were well reproduced. The dam operation was considered non-irrigation operation (equations S1 and S3), for which no sub-annual temporal variation was generated. In reality, except for the period between 1990-1992, the release tended to be high in winter and low in summer to autumn. Although such seasonality was neglected, the inter-annual change was well reproduced by the model.

2

Figure S5 (b) shows the results for the Glen Canyon Dam, which is located in the middle reach of the Colorado River in the USA. For this case, the inflow was overestimated throughout the simulation period. When a positively biased inflow is received, the model responds by releasing more water. Therefore, any overestimation in release was not attributed to the reservoir operation model but, rather, to the performance of the hydrological simulations. The model flexibly adapts to the biased inflow. The general historical variation in storage, or the decline in storage around 1990 and recovery afterwards, was well reproduced, but the storage tended to be underestimated. The release coefficient (k_{rls}) was uniformly set at 85% of the global storage capacity, but this was too low for this particular reservoir. When a higher value was set, the storage was kept high during the simulation period.

Figure S5 (c) shows the results for the Akosombo Dam, which is located in the Volta River in Ghana. For this case, the inflow was substantially overestimated throughout the simulation period, by a factor of three. The simulated storage agreed well with observations. These results can be explained by the overestimated inflow being cancelled out by releasing more water, and the k_{rls} of 85% of storage capacity being appropriate for this reservoir. This is an example of the reservoir operation sub-model adapting flexibly to the severely biased inflow, which is not avoidable in global hydrological simulations.

Figure S5 (d) shows the results for the Sirikit dam, which is located in the Chao Phraya River in Thailand. Because the primary purpose of the dam is irrigation, the daily release follows the temporal variations in water requirements in the lower reach (Eq. S2). The storage fairly well reproduced the long-term trend in storage variation and seasonality. The release showed a pattern that was high in March to May. Although it varied year by year, this generally agreed with the observations. This period corresponded to the end of the dry season or when the water requirement peaked. Due to this release pattern, the storage was lowest around May, with a large inflow during the wet season. This seasonal pattern in storage was well reproduced by the model, as were as the inter-annual fluctuations.

References

Biemans, H., Haddeland, I., Kabat, P., Ludwig, F., Hutjes, R. W. A., Heinke, J., von Bloh, W., and Gerten, D.: Impact of reservoirs on river discharge and irrigation water supply during the 20th century, Water Resour. Res., 47, W03509, 10.1029/2009wr008929, 2011.

Döll, P., and Siebert, S.: Global modeling of irrigation water requirements, Water Resour. Res., 38, 1037, 10.1029/2001WR000355, 2002.

Döll, P., Müller Schmied, H., Schuh, C., Portmann, F. T., and Eicker, A.: Global-scale assessment of groundwater depletion and related groundwater abstractions: Combining hydrological modeling with information from well observations and GRACE satellites, Water Resour. Res., 50, 5698-5720, 10.1002/2014wr015595, 2014.

Haddeland, I., Clark, D. B., Franssen, W., Ludwig, F., Voß, F., Arnell, N. W., Bertrand, N., Best, M., Folwell, S., Gerten, D., Gomes, S., Gosling, S. N., Hagemann, S., Hanasaki, N., Harding, R., Heinke, J., Kabat, P., Koirala, S., Oki, T., Polcher, J., Stacke, T., Viterbo, P., Weedon, G. P., and Yeh, P.: Multimodel Estimate of the Global Terrestrial Water Balance: Setup and First Results, J. Hydromet., 12, 869-884, 10.1175/2011jhm1324.1, 2011.

Hanasaki, N., Kanae, S., and Oki, T.: A reservoir operation scheme for global river routing models, J. Hydrol., 327, 22-41, 10.1016/j.jhydrol.2005.11.011, 2006.

Hanasaki, N., Kanae, S., Oki, T., Masuda, K., Motoya, K., Shirakawa, N., Shen, Y., and Tanaka, K.: An integrated model for the assessment of global water resources - Part 1: Model description and input meteorological forcing, Hydrol. Earth Syst. Sci., 12, 1007-1025, doi:10.5194/hess-12-1007-2008, 2008a.

Hanasaki, N., Kanae, S., Oki, T., Masuda, K., Motoya, K., Shirakawa, N., Shen, Y., and Tanaka, K.: An integrated model for the assessment of global water resources - Part 2: Applications and assessments, Hydrol. Earth Syst. Sci., 12, 1027-1037, doi:10.5194/hess-12-1027-2008, 2008b.

Hanasaki, N., Yoshikawa, S., Kakinuma, K., and Kanae, S.: A seawater desalination scheme for global hydrological models, Hydrol. Earth Syst. Sci., 20, 4143-4157, 10.5194/hess-20-4143-2016, 2016.

Kim, H., Yeh, P. J. F., Oki, T., and Kanae, S.: Role of rivers in the seasonal variations of terrestrial water storage over global basins, Geophys. Res. Lett., 36, L17402, 10.1029/2009gl039006, 2009.

5 Rost, S., Gerten, D., Bondeau, A., Lucht, W., Rohwer, J., and Schaphoff, S.: Agricultural green and blue water consumption and its influence on the global water system, Water Resour. Res., 44, W09405, doi:10.1029/2007WR006331, 2008.

Wada, Y., van Beek, L. P. H., Viviroli, D., Dürr, H. H., Weingartner, R., and Bierkens, M. F. P.: Global monthly water stress: 2. Water demand and severity of water stress, Water Resour. Res., 47, W07518, 10.1029/2010wr009792, 2011.

Wada, Y., Wisser, D., and Bierkens, M. F. P.: Global modeling of withdrawal, allocation and consumptive use of surface water
10   and groundwater resources, Earth Syst. Dynam., 5, 15-40, 10.5194/esd-5-15-2014, 2014.

Weedon, G. P., Balsamo, G., Bellouin, N., Gomes, S., Best, M. J., and Viterbo, P.: The WFDEI meteorological forcing data set: WATCH Forcing Data methodology applied to ERA-Interim reanalysis data, Water Resour. Res., 50, 7505-7514, 10.1002/2014WR015638, 2014.

15

Supplemental Tables

Table S1. Treatment of groundwater recharge, groundwater abstraction, aqueducts (or inter-cell water transfer), return flow and delivery loss, reservoirs, and desalination in four global hydrological models (GHMs) used for assessing human water abstraction.

Model	**WaterGAP**	**PCR-GLOBWB**	**LPJmL**	**H08**
References	Döll et al. (2014)	Wada et al. (2014)	Rost et al. (2008) Biemans et al. (2011)	This study
Groundwater recharge	Empirically estimated from total runoff of the surface soil layer.	Estimated from the soil moisture content and hydraulic conductivity of the second soil layer (S2) and third groundwater layer (S3). Recharge equals deep percolation (S2) minus capillary rise (S3).	Not included in the model.	Same as WaterGAP
Groundwater abstraction	Taking water from the renewable groundwater reservoir. If it is depleted, excess abstraction is allowed.	Taking water from the renewable groundwater reservoir. If it is depleted, excess abstraction is allowed. If reservoirs are present, surface water abstraction is preferred.	Not included in the model	Same as WaterGAP.
Fractional contribution of groundwater to total water abstraction	Fixed by statistical data.	Assumed to be proportional to the fraction of baseflow to total runoff, but it is flexible because surface water is preferred when reservoirs are present, and groundwater is additionally used when surface water is depleted until it reaches the value reported in IGRAC (2004).	Not applicable.	Same as WaterGAP

Aqueducts or inter-cell water transfer	If local surface water sources are depleted, water is taken from the neighboring cells with the largest catchment area.	Not included in the model.	If local surface water sources are depleted, water is taken from neighboring cells with the largest discharge.	If river flow is depleted, water is taken from nearby grid-cells through explicit (representing the actual aqueducts) and implicit (inferred by the geographical conditions) aqueducts.
Return flow	Not calculated in the hydrological simulation. Water for consumption is abstracted from water sources.	Calculated for irrigation, industrial, and municipal water abstraction	Calculated for irrigation water use.	Calculated for irrigation, industry, and municipal water abstraction.
Delivery loss	Not included in the model	Calculated for irrigation water use. By their definition, industrial and municipal water consumption included leakage.	Calculated for irrigation water use. Assumed to be 50% of return flow.	Same as LPJmL
Reservoir classification	Not applicable. Storage capacity of reservoirs was accumulated for each cell and treated as a single reservoir on the main channel.	Same as WaterGAP	Same as WaterGAP.	Reservoirs with a catchment area exceeding 5000 km^2 regulate the streamflow of the global river network. Remaining reservoirs are aggregated into one for each cell, which is isolated from the global river network.
Seawater desalination	Not included in the model.	The reported volume of seawater desalination is allocated along the coastline as an available water source.	Not included in the model.	The area utilizing seawater desalination (AUSD) was estimated by the algorithm of Hanasaki et al. (2016). The volume was estimated by the local water supply and demand balance.

Table S2 Regional classification of Giorgi and Francisco (2000).

Region	Abbreviation
Australia	AUS
Amazon Basin	AMZ
Southern South America	SSA
Central America	CAM
Western North America	WNA
Central North America	CAN
Eastern North America	ENA
Alaska	ALA
Greenland	GRL
Mediterranean Basin	MED
Northern Europe	NEU
Western Africa	WAF
Eastern Africa	EAF
Southern Africa	SAF
Sahara	SAH
Southeast Asia	SEA
East Asia	EAS
South Asia	SAS
Central Asia	CAS
Tibet	TIB
North Asia	NAS

Table S3 The river discharge and terrestrial water storage anomaly (TWSA) simulations for less heavily human-affected basins. NSE and CC for Nash-Sutcliffe efficiency and correlation coefficient, respectively

River	River discharge				TWSA						
	NSE		Bias		NSE		CC		Slope [mm yr^{-1}]		
	NAT	ALL	NAT	ALL	NAT	ALL	NAT	ALL	NAT	ALL	GRACE
Amazon	0.67	0.68	0.05	0.05	0.74	0.75	0.88	0.88	-0.68	-0.61	3.70
Congo	-17.51	-17.48	0.92	0.92	-0.29	-0.29	0.55	0.55	0.85	0.86	-0.92
Yenisei	0.43	0.42	-0.32	-0.32	0.39	0.36	0.67	0.65	-1.21	-1.77	1.39
Ob	0.62	0.57	0.14	0.14	0.37	0.35	0.71	0.69	-2.03	-1.81	-3.88
Lena	-0.01	-0.01	-0.35	-0.35	-0.02	-0.04	0.46	0.46	0.21	-0.02	1.55
Amur	0.21	0.18	-0.22	-0.25	0.02	0.03	0.54	0.57	4.80	5.57	2.99
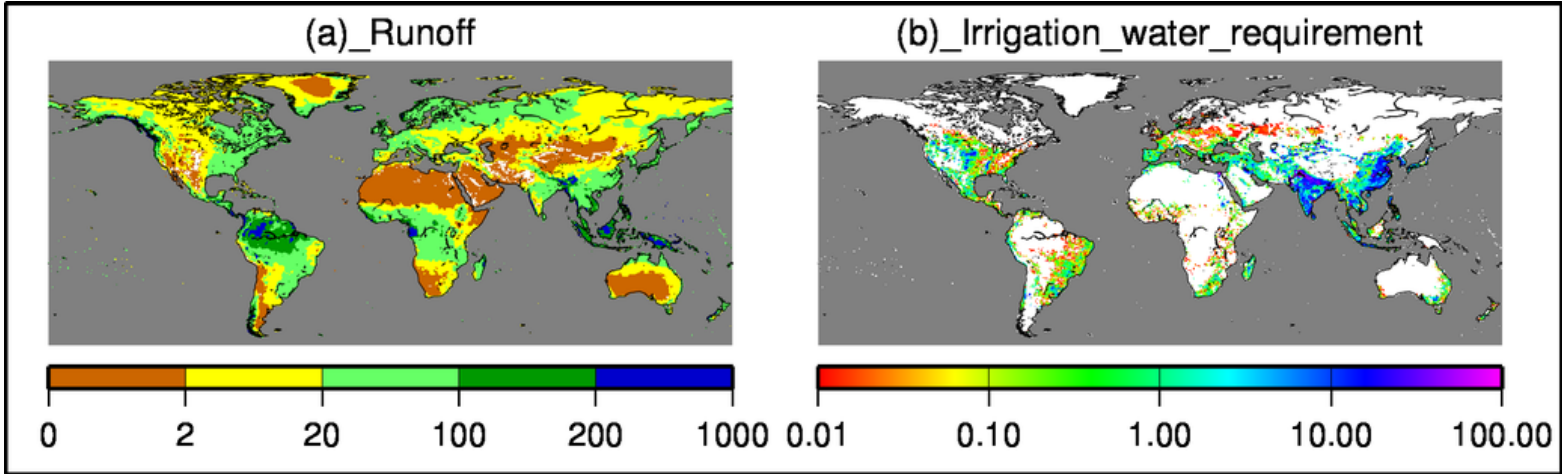
Figure S1 Global distribution of mean annual (a) runoff [kg m^{-2} yr^{-1}] and (b) irrigation water requirement [m^3 s^{-1}].
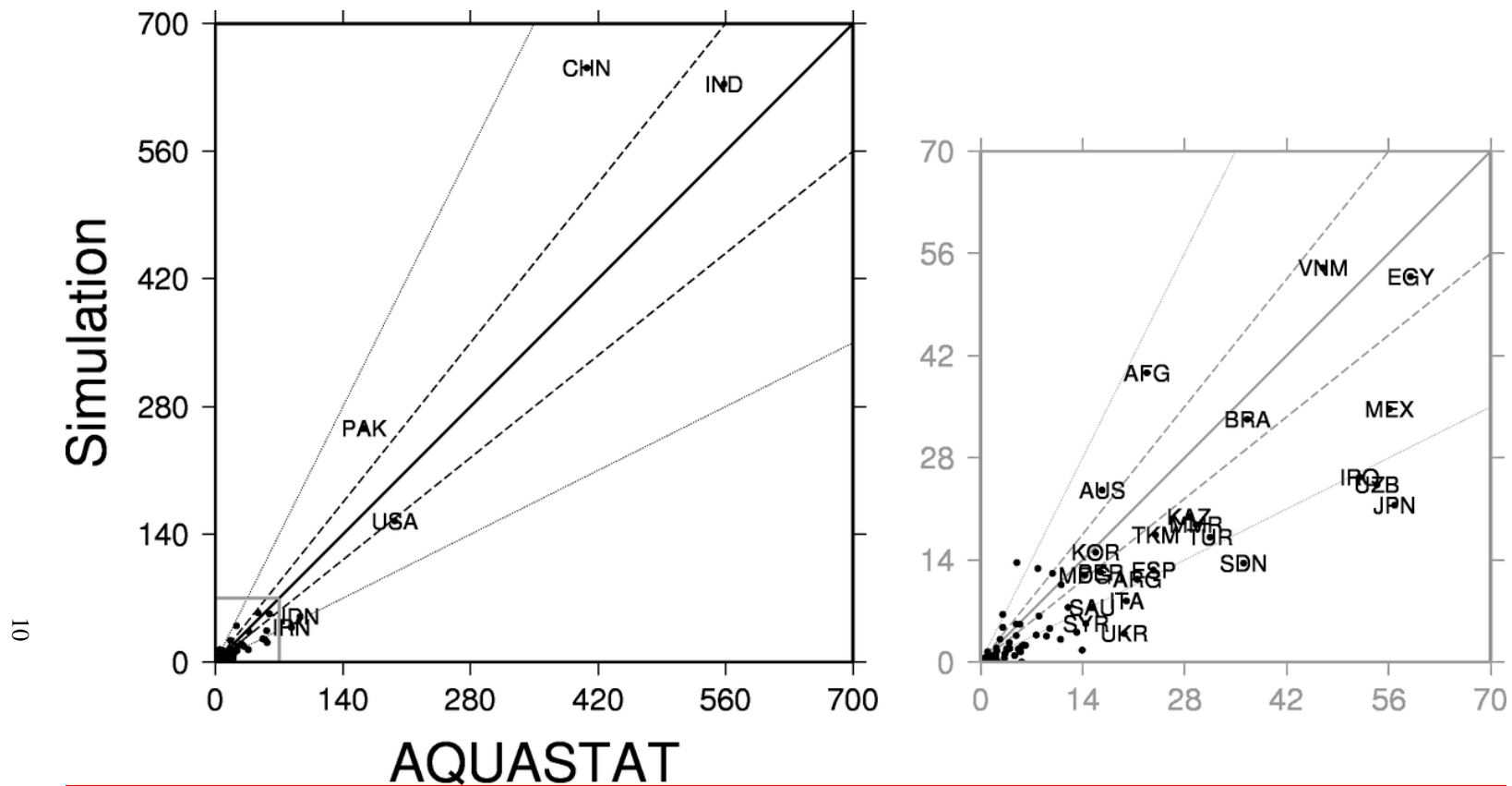
Figure S2 National estimates of annual irrigation water withdrawal (km^3 yr^{-1}). The panel in gray is an enlargement of part of the original figure.
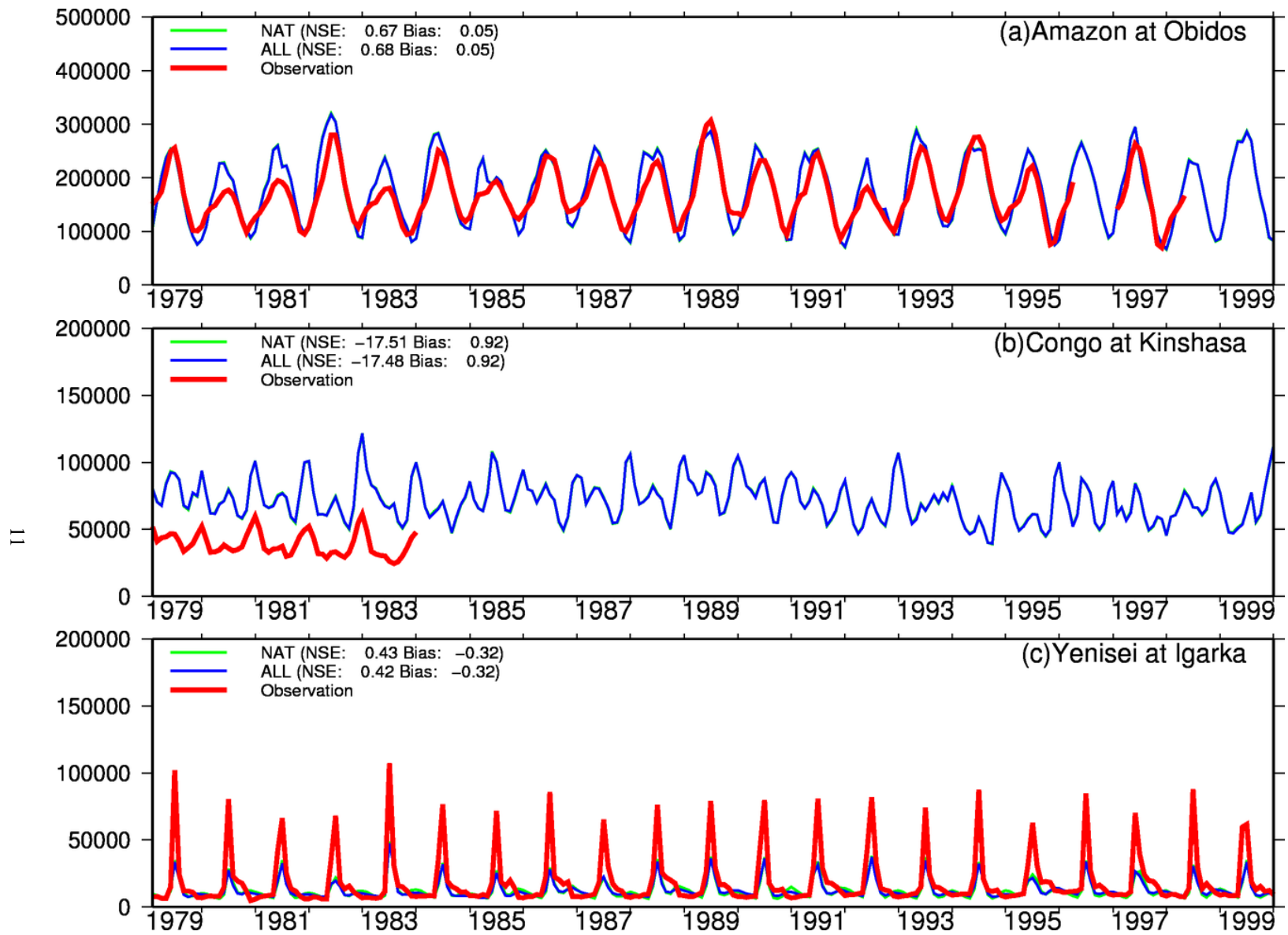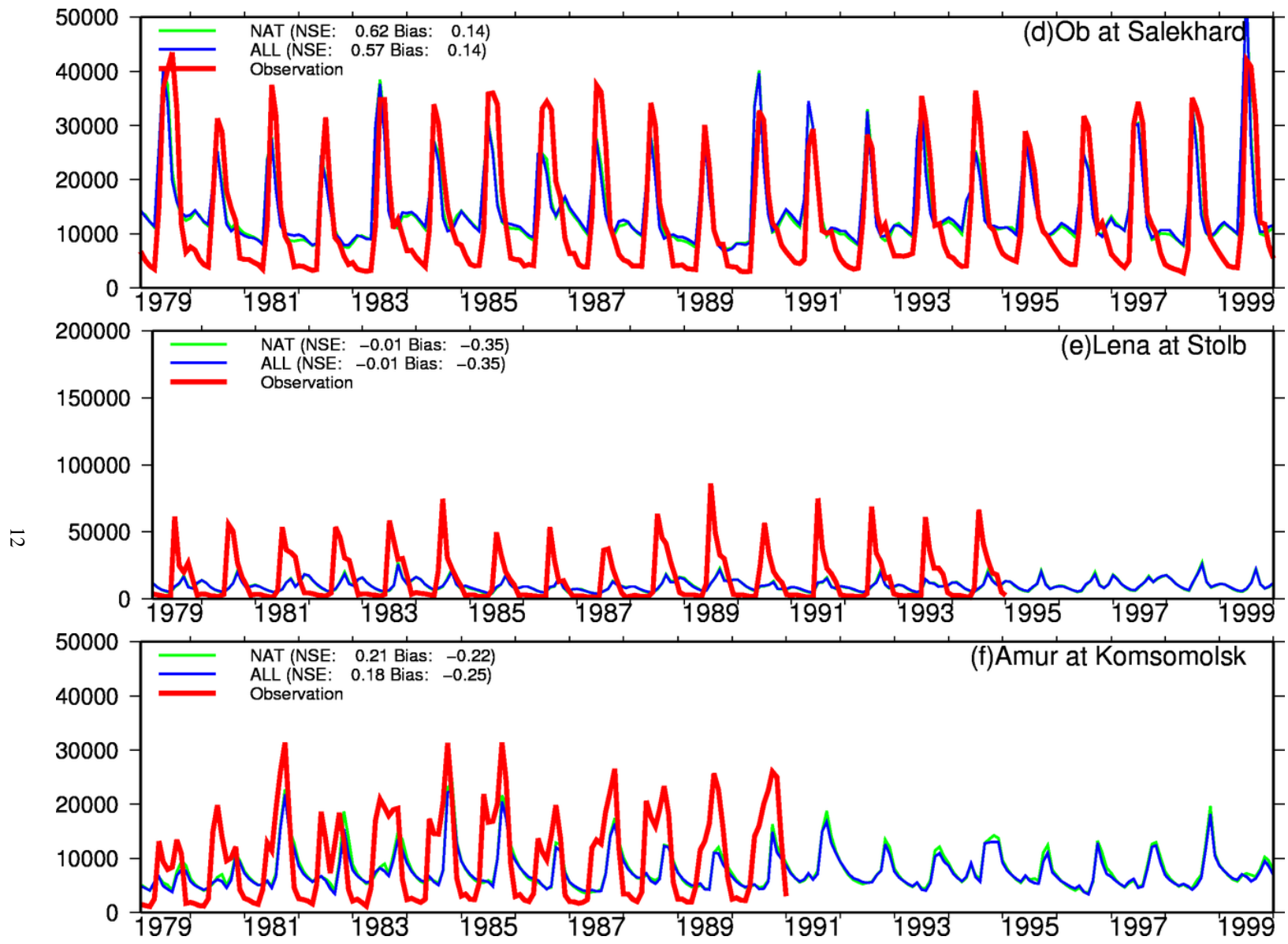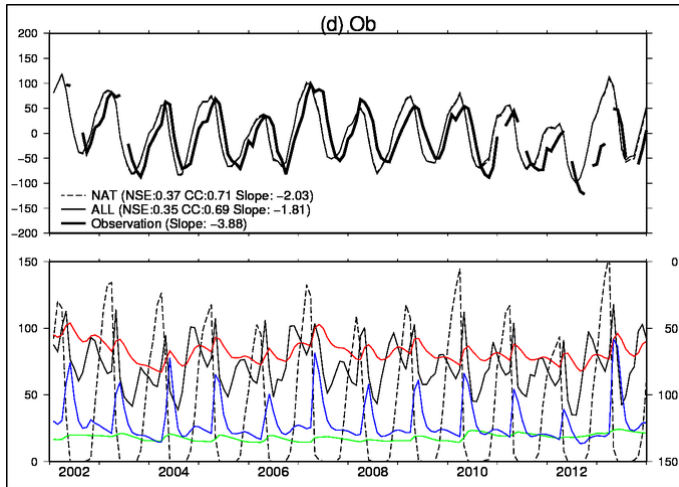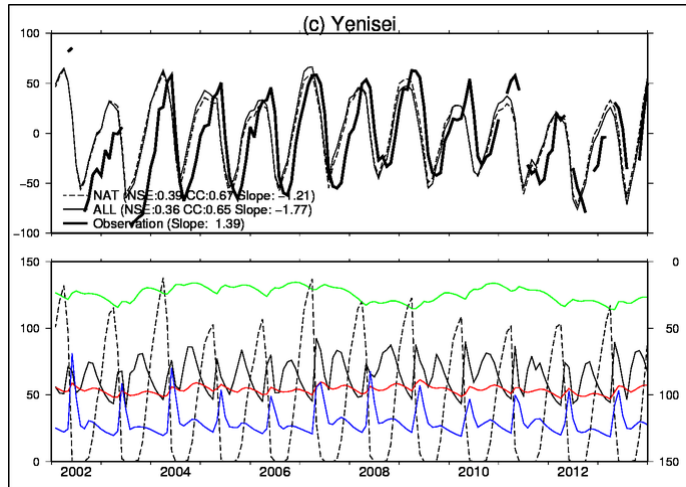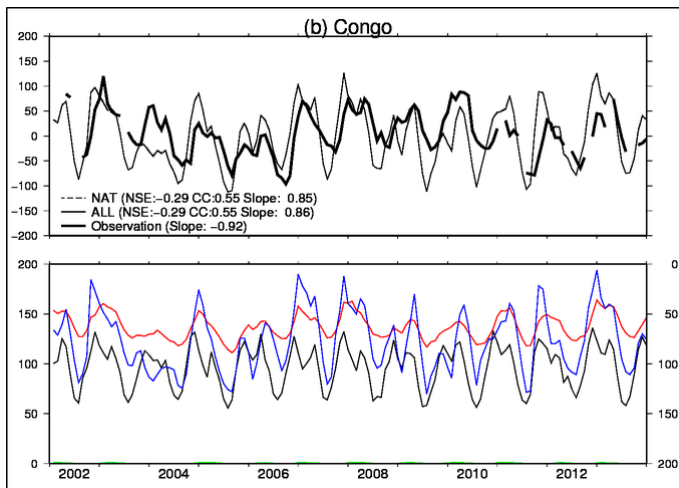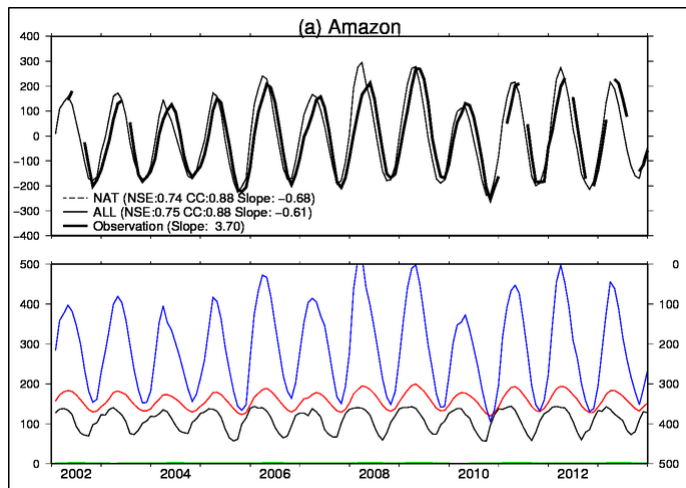
Figure S3 River discharge at six less heavily human-affected basins: (a) The Amazon River at Obidos, (b) the Congo at Kinshasa, (c) the Yenisei River at Igarka, (d) the Salekhard River at Ob, (e) the Lena River at Stolb, and (f) the Amur River at Komsomolsk.
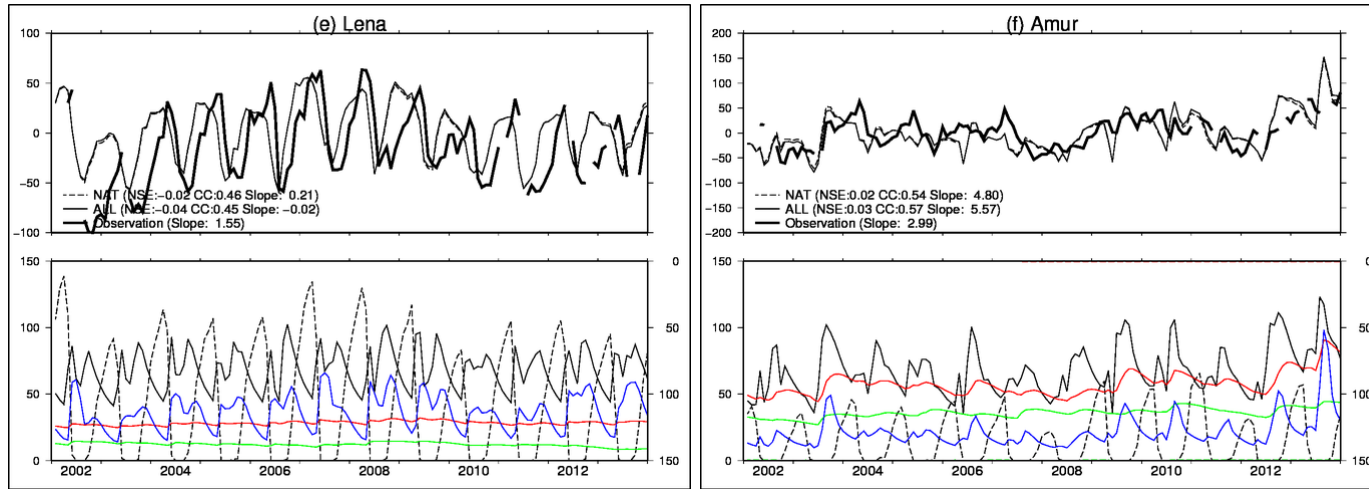
5

Figure S4 Terrestrial water storage (TWS) of six less heavily human-affected basins. The top panel of each figure shows the terrestrial water storage anomaly (TWSA) [mm]. The bold and thin lines show the GRACE observation and the H08 simulation, respectively. The bottom panel of each figure shows the simulated terrestrial water storage components [mm]: solid black (soil moisture), broken black (snow water), solid red (renewable groundwater), broken red (cumulative volume of nonrenewable groundwater abstraction; right axis), solid green (storage in global reservoirs), broken green (storage in local reservoirs), and solid blue (river water). Note the sign of the cumulative volume of nonrenewable groundwater abstraction, where a positive sign denotes a decrease in water volume.
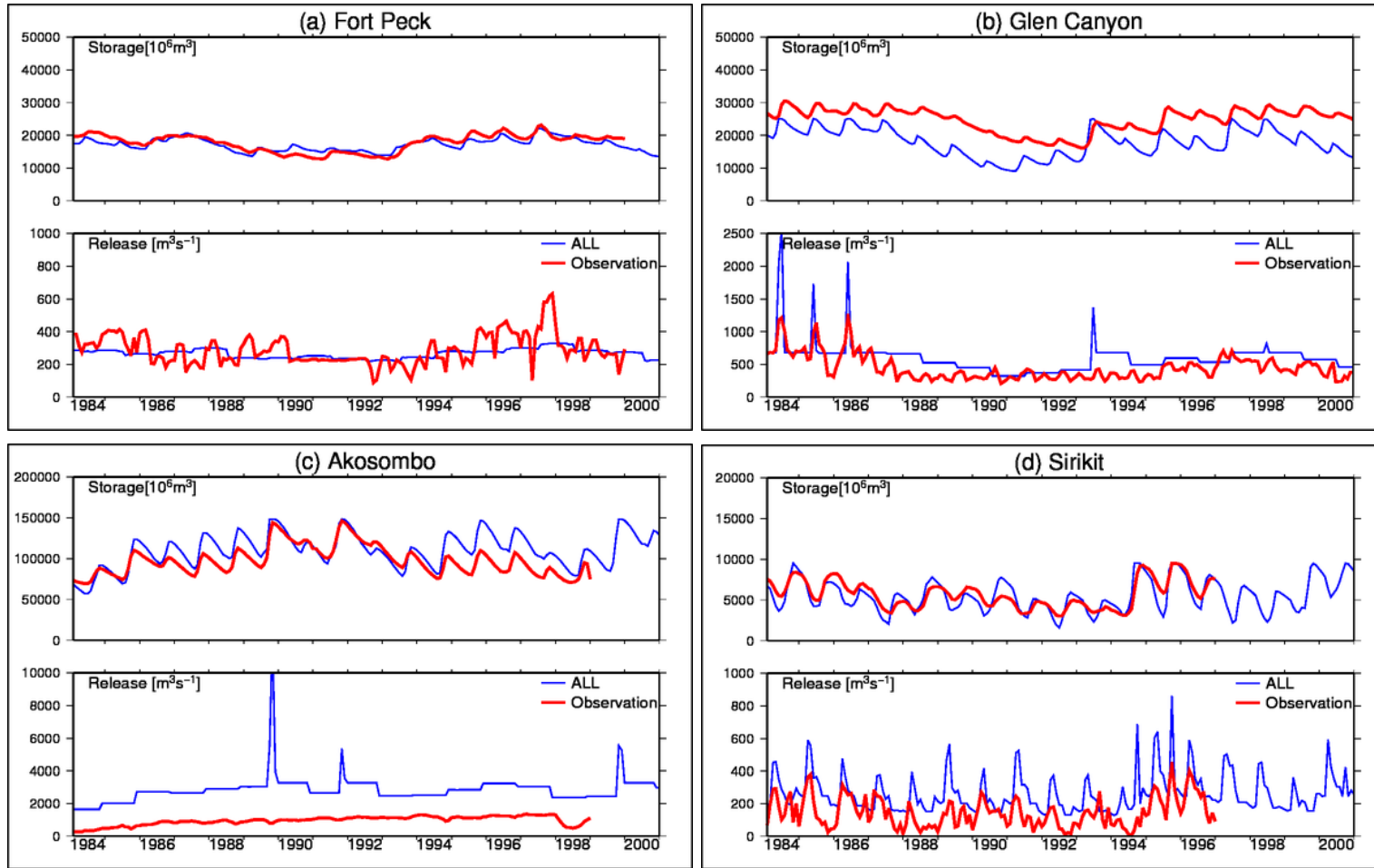
Figure S5 Reservoir operation at four of the world's major reservoirs. (a) Fort Peck Dam on the Missouri River (Mississippi River), (b) Glen Canyon Dam on the Colorado River, (c) Akosombo Dam on the Volta River, and (d) Sirikit Dam on the Chao Phraya River.